Terahertz plasmonic composites

Syrus C. Nemat-Nasser,[1,*] Alireza V. Amirkhizi,[1] Willie J. Padilla,[2,†] Dimitri N. Basov,[2] Sia Nemat-Nasser,[1,‡] Derek Bruzewicz,[3] and George Whitesides[3]

[1]*Center of Excellence for Advanced Materials, Department of Mechanical and Aerospace Engineering, University of California, San Diego, Mail code: 0416, 9500 Gilman Drive, La Jolla, California 92093-0416, USA*

[2]*Department of Physics, University of California, San Diego, Mail code: 0416, 9500 Gilman Drive, La Jolla, California 92093-0416, USA*

[3]*Department of Chemistry and Chemical Biology, Harvard University, Cambridge, Massachusetts 02138, USA*

(Received 27 October 2006; revised manuscript received 20 December 2006; published 27 March 2007)

The dielectric response of a polymer matrix composite can be substantially modified and tuned within a broad frequency band by integrating within the material an *artificial plasmon medium* composed of periodically distributed, very thin, electrically conducting wires. In the microwave regime, such plasmon/polymer composites have been studied analytically, computationally, and experimentally. This work reports the design, fabrication, and characterization of similar composites for operation at terahertz frequencies. Such composites require significant reduction in the thickness and spacing of the wires. We used numerical modeling to design artificial effective plasmonic media with *turn-on frequencies* in the terahertz range. Prototype samples were produced by lithographically embedding very thin gold strips into a PDMS [poly(dimethylsiloxane)] matrix. These samples were characterized with a Fourier-transform infrared interferometer using the frequency-dependent transmission and Kramers-Kronig relations to determine the electromagnetic properties. We report the characterization results for a sample, demonstrating excellent agreement between theory, computer design, and experiment. To our knowledge this is the first demonstration of the possibility of creating composites with tuned dielectric response at terahertz frequencies.

DOI: 10.1103/PhysRevE.75.036614 PACS number(s): 42.25.Bs, 42.70.−a, 73.20.Mf

I. INTRODUCTION

Structured conducting media referred to as artificial dielectrics have been studied since the 1950's, and perhaps earlier, for modeling RF propagation in the ionosphere. Due to low intrinsic losses, these artificial media have also been considered for use as microwave lenses [1,2]. Many artificial dielectrics are plasma analogs that we refer to as *artificial plasmon media*. These media share an interesting characteristic: they dramatically affect electromagnetic radiation while occupying a small, often negligible volume fraction. Due to this characteristic, artificial plasmon media can be embedded into structural composites resulting in large scale changes in the bulk electromagnetic response without significantly degrading structural integrity.

In 1996, Pendry *et al.* [3] examined the effective electromagnetic properties of an artificial plasmon medium composed of a periodic arrangement of very thin, conducting wires, and predicted a plasma frequency in the microwave regime, below the diffraction limit. Following this work, it was experimentally established [4] that embedding a regular array of very thin wires within an insulating host material alters the dielectric response to a suitably polarized electromagnetic radiation such that

$$\kappa = \kappa(f) \cong k - \frac{f_p^2}{f^2}. \tag{1}$$

Here, κ is the effective dielectric constant of the composite with the embedded wire array; f is the frequency of the electromagnetic radiation; k is the dielectric constant of the host material; and f_p is a *plasma frequency* that depends only on the properties of the embedded wire array. In case of a uniaxial array of wires, the suitable polarization must be parallel to the array. For an ideal plasma, i.e., for $k=1$ in Eq. (1), the plasma frequency defines a threshold below which no electromagnetic radiation can propagate and above which the dielectric constant asymptotically approaches 1 as $f \to \infty$. At microwave frequencies, an array of very thin copper wires simulates the response of an ideal plasma [3,4].

For an artificial plasmon medium embedded in a host material with dielectric constant k, we define a *turn-on* frequency f_t as

$$f_t \equiv \frac{f_p}{\sqrt{k}}. \tag{2}$$

This frequency is the lowest at which nonevanescent electromagnetic waves can propagate through the composite. Pendry *et al.* [3] showed that the plasma frequency f_p for a regular three-dimensional cubic lattice of very-thin, very-long cylindrical wires can be estimated according to

$$f_p^2 = \frac{1}{2\pi}\left(\frac{c^2/d^2}{\ln(d/r) - \frac{1}{2}(1 + \ln \pi)}\right), \tag{3}$$

where d is the lattice spacing, r is the wire radius, and c is the speed of light in vacuum. Equation (3) is valid for choices of d and r that result in a wavelength λ_p at the

*Present address: Fair Isaac Corporation, 3661 Valley Centre Drive, San Diego, CA 92130.

†Present address: Department of Physics, Boston College, Chestnut Hill, MA 02467.

‡Corresponding author. Electronic address: sia@ucsd.edu

plasma frequency that is significantly larger than the lattice spacing, i.e.,

$$\lambda_p = \frac{c}{f_p} \gg d. \tag{4}$$

Equation (4) is a basic design constraint. Previous designs [4] of structural composites with modified dielectric constant at microwave frequencies required wires with diameters on the order of 10^{-5} m. Our present work demonstrates that, by scaling this dimension down to nanometers, one can achieve plasma frequencies in the terahertz regime.

A great amount of work has been done previously on the interaction of metallic grids, meshes, and other periodic arrays with electromagnetic waves in the far infrared regime. Ulrich [5–7] extensively studied various designs that create low-pass, high-pass, band-pass, and stop-band filters. Before these pioneering works, the infrared filters were constructed by stacking of quarter-wavelength-spaced layers of various dielectrics, that involve some processing difficulties. More recently, Smith *et al.* [8] have also studied these stacked filter designs. Puscasu *et al.* [9] measured the transmission and reflection from frequency selective surfaces consisting of a single layer of a two-dimensional (2D) periodic array of isolated or coupled dipoles. Wu *et al.* [10] have measured the reflectance of a multiple layer thin wire array. In a later work, Yen *et al.* [11] measured the transmission of gold deposited PDMS layers and studied the change in the turn-on frequency as a function of the spacing as the elastomeric PDMS substrate is stretched. The present paper differs from these cited works in that we consider the composite samples as effective media and directly extract their overall material properties from experimental measurements. Moreover, we present unique techniques for manufacturing of such composite samples. We also obtain excellent agreement between our numerical predictions, based on which the samples have been designed and constructed, and our experimental measurements.

II. NUMERICAL ANALYSIS AND DESIGN

Numerical simulations of Maxwell's equations were used to design a heterogeneous microstructure for terahertz-frequency-range plasmonic composites, subject to sample production constraints. We used two software packages for numerical simulation: (i) Ansoft-HFSS [12], a commercial finite-element electromagnetic solver, capable of modeling various boundary conditions in the complex-valued frequency domain; (ii) GdfidL [13], an electromagnetic solver developed by Dr. Warner Bruns. These packages were used to calculate the resonance frequencies of unit cells of assumed periodic configurations. All terahertz-regime simulations were conducted using HFSS.

Consider a Bloch wave traveling in the x direction in a three-dimensionally periodic structure. We are interested in an effective response that corresponds to macroscopic plane-wave propagation. Electromagnetic field values are thus periodic in the y and z directions, having a period equal to the corresponding size of the unit cell

$$\mathbf{F}(x, y = y^+, z) = \mathbf{F}(x, y = y^-, z),$$

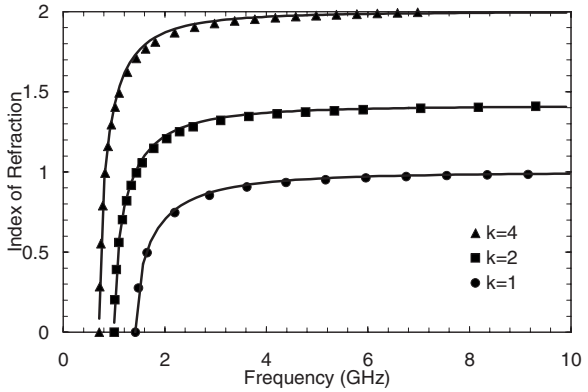

FIG. 1. Agreement between theory and numerical simulation in predicting the index of refraction versus frequency of a plasmon/polymer composite in the absence of electromagnetic losses. Symbols indicate the results of numerical simulations using GdfidL [13] for a matrix dielectric constant k of 1, 2, and 4; solid lines indicate the Eq. (1) model where the index n is computed as the square of the effective dielectric constant κ. Both the dielectric matrix and the artificial plasmon medium were treated as lossless, i.e., the loss tangent was zero for the dielectric, and all metals were treated as perfect conductors.

$$\mathbf{F}(x, y, z = z^+) = \mathbf{F}(x, y, z = z^-). \tag{5}$$

Here $\mathbf{F}$ is any of the electromagnetic field quantities, $\mathbf{E}$, $\mathbf{H}$, $\mathbf{D}$, or $\mathbf{B}$. The x-direction period is defined by the wavelength of the traveling electromagnetic radiation. The effective medium assumption requires a wavelength significantly greater than the size of the unit cell in the x dimension. A monofrequency sinusoidal wave of such wavelength has a small phase advance across the cell. This prescribes the required boundary conditions for the unit cell as follows:

$$\mathbf{F}(x = x^+, y, z) = \mathbf{F}(x = x^-, y, z)e^{i\varphi},$$

$$\varphi = \frac{2\pi}{\lambda} d. \tag{6}$$

The phase advance φ is determined by the wavelength λ and the cell size $d = x^+ - x^-$. A unit cell with these periodic boundary conditions is geometrically modeled using numerical simulations, and treated as a cavity with a resonance frequency $f(\varphi)$ that can be calculated for different values of the phase advance φ. This frequency $f = f(\varphi)$ can be interpreted as the frequency at which a wave, with wavelength λ, travels

TABLE I. Comparison of the analytical prediction due to Pendry *et al.* [3] and numerical simulation for the plasma frequency of an array of thin wires at very short wavelengths.

Wire spacing (μm)	Analytical prediction (GHz)	HFSS simulation (GHz)
10	8630	8940
50	1275	1325
75	804	833
100	582	605

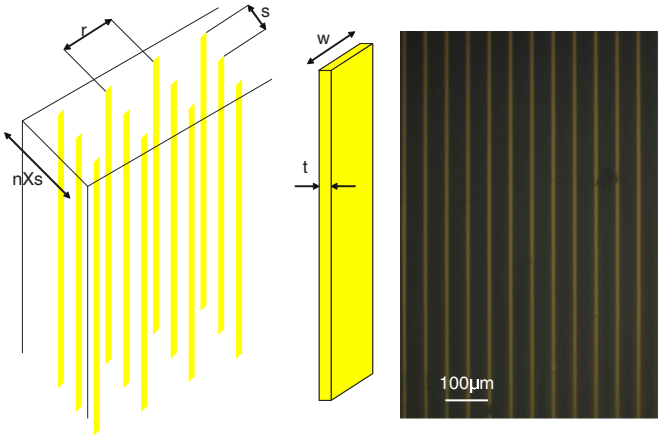

FIG. 2. (Color online) The micron-scale thin strip array. Left: The slab of n rows of strips spaced r in-plane and s through the thickness. Center: A single strip of width w and thickness t. Right: Optical micrograph of an array of thin gold strips in PDMS.

through the medium. The corresponding dispersion relation is as follows:

$$f_{resonance}(\varphi) = f(\lambda) = \frac{v_p(f)}{\lambda} = \frac{c/n(f)}{\lambda},$$

$$n(f) = \frac{c}{\lambda f(\lambda)} = \frac{c\varphi/2\pi}{df_{resonance}(\varphi)}. \quad (7)$$

Here $v_p(f)$ and $n(f)$ are the phase velocity and the index of refraction at f, respectively; and c is the speed of light in vacuum. Note that in the absence of any magnetic behavior, it can be assumed that the effective dielectric constant κ is related to the index of refraction by $\kappa = n^2$.

We have used this method successfully to design a number of composites with tuned dielectric constants in the microwave regime. Figure 1 presents some simulation results using GdfidL to demonstrate the agreement between the analytical prediction of Eq. (1) and direct numerical simulation. Table I compares the Eq. (3) prediction for the plasma frequency with HFSS numerical calculations for an array of 1-μm diameter copper wires. The HFSS numerical simulations include finite electromagnetic skin-depth effects for copper, whereas the analytical formula and GdfidL simulations assume perfect conductors. The close agreement between analysis and simulation suggests that an effective plasmonic response should be observed at terahertz frequencies.

In general, the cross-sectional shape of the wires is not as important as their cross-sectional area. Therefore, the fabrication process can be simplified by using thin strips instead of round wires. Geometric parameters are defined in Fig. 2 and Table II for two sets of specimens, denoted as Set 1 and Set 2. The last three columns in Table II report the predicted *turn-on*, *match*, and *diffraction-limit* frequencies, respectively. The turn-on frequency, defined in Eq. (2), was discussed previously. The *match frequency* is defined as the frequency at which the effective dielectric constant and the index of refraction are both equal to unity. One can consider a band around the match frequency, in which the index of refraction deviates from 1 by a desired limit; say 10%. In this band, the lensing effect of the composite is limited. Therefore, in this band, the structure would minimally interfere with the transmission of the electromagnetic waves such as communication signals. The *diffraction-limit frequency* is the frequency at which the electromagnetic wavelength is equal to twice the array wire spacing. The frequency band between the turn-on frequency and the diffraction limit is where the composite can be homogenized and considered "transparent;" that is, electromagnetic (EM) waves can be transmitted through the thickness of the sample with small losses. Below the turn-on frequency, the imaginary part of the index of refraction becomes significant, weakening the transmitted waves substantially, due to large impedance mismatch and very lossy medium. Above the diffraction limit, one cannot define homogenized material properties, since then the wavelength would be of the same order of magnitude as the length of the microstructural elements. Both sets of our specimens consist of gold nanostrips plated on the surface of (Set 1) or embedded within (Set 2) poly(dimethylsiloxane) (PDMS) that has a dielectric constant of about 2.4 in the range of the frequencies studied here; see Fig. 3.

III. FABRICATION METHOD

Composite samples were prepared using *e*-beam evaporation of gold onto membranes of poly(dimethylsiloxane) (PDMS; Sylgard 184, Dow Corning, Midland, MI). The PDMS membranes were prepared by spinning a degassed mixture of prepolymer and catalyst on silanized wafers. After curing, the PDMS was oxidized and then spin coated by a 5 μm thick layer of photoresist.[1] Via photolithography with a chrome mask, we identified the inverse of the desired pattern for producing samples with 2.5 or 5 μm wide metal strips spaced by 25 or 50 μm center-to-center, respectively (see Fig. 2 and Table II). Using a Temescal CV-8 electron-beam evaporator, a 2-nm layer of titanium was deposited, followed by gold. To prevent buckling of the PDMS [14], the samples were cooled during evaporation by filling a dewar embedded in the top of the evaporation chamber with liquid nitrogen. The evaporation proceeded in 10-nm intervals, with a 10 min pause between each interval, also to prevent overheating and buckling. The photoresist was removed and the patterns of gold lines were revealed by immersing the sample in 100% ethanol and sonicating gently for 5–10 min [15].[2]

The multilayer arrays of gold lines were fabricated by spin-coating additional layers of PDMS and repeating the process described above. The fully embedded metal strips were produced by spin-coating and curing a final layer of PDMS on the sample. Then the samples were peeled away from the silicon support with tweezers. The resulting membranes are asymmetric, as the depth of the PDMS layer cov-

[1]Instead of baking the photoresist, it was allowed to sit at room temperature for 30 min; baking caused cracks in the photoresist, due to the different coefficients of thermal expansion of the photoresist and the PDMS.

[2]Acetone is usually used to remove Shipley resists, but swells PDMS; see Lee *et al.* [15].

TABLE II. Dimensions (all in μm) of the PDMS-Gold strip composites, and the corresponding turn-on, match, and diffraction limit frequencies entries (in THz).

Set	r	s	w	t	n	Turn-on	Match	Limit
1	50	100	5	0.1, 0.2, 0.3 (0.2 simulated)	1	0.67	0.80	0.95
2	25	20	2.5	0.2	1, 2	2.37	3.10	4.74

ering the metal strips on one side is twice that of the other side.

To simplify handling and measurements, samples were studied while mounted on black nylon sample holders. Each sample holder consisted of two 5 mm thick nylon discs bolted together, with holes drilled to allow light to pass. The composite membranes were mounted by first wetting the inner surface of one disc with 100% ethanol, and then sliding the membrane—free from its silicon support—over the ethanol. Capillary action kept the membrane flat, and the ethanol acted as a lubricant between the membrane and the nylon. After positioning the sample in the desired orientation over a hole, the excess ethanol was wicked away, the remaining solvent was allowed to evaporate, and the sample holder was screwed together to lock the sample in place.

IV. MEASUREMENT

All measurements were carried out under vacuum using a commercially available Fourier-transform interferometer. A silicon bolometer cooled to liquid helium temperatures was used as the detector; the light source for the measurements was a mercury arc lamp, and a germanium-coated Mylar beam splitter was used within the interferometer for the frequency range of interest. Measurements of the polymeric composites were performed with polarized light since the samples characterized were all uniaxial.

As described above, the wires are plated on the surface of (Set 1) or embedded within (Set 2) a PDMS matrix, and a characterization of the polymer matrix was carried out in order to determine its optical properties. The absolute values of both transmission and reflection were measured for 400 μm thick PDMS from about 1 to 20 THz as follows. We first measured the transmission through a PDMS sample via a 3 mm aperture normalized by the transmission through the open aperture. The reflectance of the same sample at near normal incidence was measured and then referenced by the reflectance from a perfectly reflecting material, i.e., a terahertz mirror. The measured coefficients, $T(f)$ and $R(f)$, were then inverted using a program written in Mathematica. The results for the real, $\kappa_1(f)$, and imaginary, $\kappa_2(f)$, parts of the dielectric response for the PDMS sample are shown in Fig. 3. Note that our analysis up to this point has ignored the imaginary, absorptive part of κ. The data presented in Fig. 3 indicates a loss tangent (the ratio of the imaginary part of the dielectric constant to its real part) between 0.01 and 0.05 in the frequency range depicted in Fig. 5.

With the complex dielectric function of the host material characterized, $T(f)$ was measured for the polymeric composite materials. The samples were placed behind a 3 mm aperture. The power transmitted through the sample was measured. The ratio of this value to the power transmitted through an open aperture is used in the calculations. The sample holder was attached to a piezoelectric rotational stage which is accurate to within 0.5°. Figures 4 and 5 present the absolute transmission and dielectric response for one of the samples, respectively. In the following section, we describe the method used to determine the dielectric response.

V. MATERIAL PARAMETER EXTRACTION

In general, to evaluate the complex-valued electric permittivity, $\tilde{\varepsilon}(\omega)=\varepsilon_1(\omega)+i\varepsilon_2(\omega)$ and magnetic permeability, $\tilde{\mu}(\omega)=\mu_1(\omega)+i\mu_2(\omega)$ four real-valued frequency-dependent measurements are required (here $\omega=2\pi f$ is the angular fre-

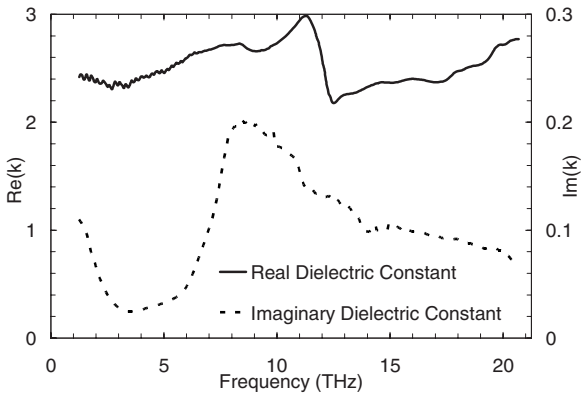

FIG. 3. Measured dielectric response of the PDMS matrix. From 1 to 6 THz, the dielectric constant is approximately equal to 2.4 with a loss tangent between 0.01 and 0.05.

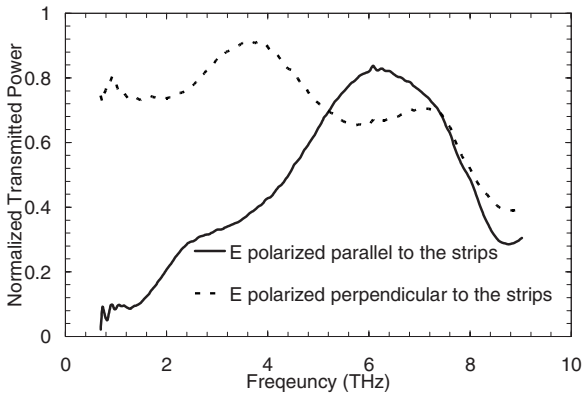

FIG. 4. Measured normalized transmitted power for two polarizations of the electric field through the single-layer sample from Set 2.

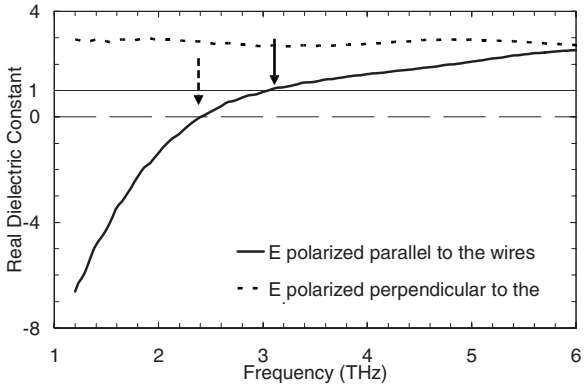

FIG. 5. The extracted dielectric constant of the single-layer sample of Set 2 from Kramers-Kronig relations. The dashed arrow indicates the numerically predicted turn-on frequency of 2.37 THz, and the solid arrow indicates the predicted match frequency of 3.10 THz; see Table II. These can be compared visually to where the measured value of the normalized dielectric constant crosses zero (turn-on) and where it crosses one (match).

quency). Alternatively, $T(\omega)$ and $R(\omega)$, the complex transmission and reflection coefficients, may be measured over all frequencies, and the phase for each may be calculated using the Kramers-Kronig integral relation. Then the complex transmission and reflection coefficients may be utilized to calculate the optical constants, i.e., $\tilde{\varepsilon}(\omega), \tilde{\mu}(\omega)$ [16,17]. In the present study, the required measurement was simplified by taking the effective magnetic permeability of the polymeric composite to be equal to that of free space, since the magnetic activity of the thin wire array is negligibly small. Thus, two real-valued measurements are required to extract the complex-valued dielectric constant. In the present analysis, this is achieved by utilizing an inversion technique previously detailed by Singley *et al.* [18]. Since the membrane is asymmetric through its thickness, it is modeled as a symmetric composite (gold strips symmetrically embedded within a PDMS matrix) on a layer of PDMS substrate. This substrate is located on the transmission side. The measured power includes the effect of the substrate. To extract the material properties of the composite, we need to calculate the *corrected* transmitted signal as it exits the composite. This can be achieved by using the known material properties of the substrate and a simple algebraic calculation detailed in [18]. The Kramers-Kronig integral relations are then used for the corrected transmission to obtain the phase $\theta(\omega)$ of the transmitted wave [17,18]. The Kramers-Kronig method requires transmission over the full infinite frequency domain. Therefore, function $T(\omega)$ is extrapolated based on physical assumptions and the existing constraints. For the high-frequency limit in the complex plane, $|\omega| \to \infty$, it is required that $\ln|T(\omega)| = o(|\omega|^{\alpha})$, where $0 < \alpha < 1$, ensuring that $T(\omega) \to 0$ and that the Kramers-Kronig integral is bounded. For the low-frequency limit, $|\omega| \to 0$, we consider two cases. For plasmonic composites (low frequency stop band), we extrapolate so that $T(\omega) \to 0$. In the absence of a low frequency stop band, $T(\omega)$ is extrapolated to the transmission limit of the matrix material. Note that the calculated $\theta(\omega)$ requires an additive correction, $A\omega$, to correct for the extrapolations [18], where A is a slowly varying function of frequency that can be approximated by a constant. To find the value of A, we note that for frequencies close to the diffraction limit (away from the plasmon frequency), the optical properties of the composite must approach those of the matrix. This and the low-frequency assumption (in the absence of a stop band) are justified, since the volume fraction of the conductor is very small (10^{-3}) and its effect is negligible away from the plasmonic resonance or in a nonplasmonic medium. For more detail of the calculation of the Kramers-Kronig integrals and the significance of these assumptions (smooth extrapolation of $T(\omega)$ beyond the measurement range and the corrections to $\theta(\omega)$), see the Appendix. The dielectric function is now determined from $T(\omega)$ and $\theta(\omega)$, based on the impedance theory [19]. Note that, since the transmission equations have multiple branches of solution for the dielectric function, direct inversion of these equations would not be useful. Instead, we use an iterative search method to find $\tilde{\varepsilon}(\omega)$, starting from its known value for the next higher frequency, $\tilde{\varepsilon}(\omega+\Delta\omega)$, where $\Delta\omega$ is the frequency step size. For the highest frequency, we use the properties of the PDMS for the starting point, as one expects that the material properties of the composite approach that of the PDMS at this limit.

VI. RESULTS

The results of our measurements are shown in Figs. 4 and 5. Two measurements were taken on the same single-layer sample from Set 2, one with the electric field polarized in the direction of the wires, and the other with the electric field polarized normal to the wires; see Figs. 4 and 5. A slab of homogenous material with the equivalent effective dielectric constant depicted in Fig. 5 has the same transmission and reflection properties as the sample. The thickness of the slab is defined as the periodicity of the medium. The effective medium is defined for a large number of layers. However, as discussed in Sec. VII, the measured overall properties are essentially the same for 1, 2, or 3 layers and also agree with numerical predictions for infinite number of layers. The effective plasmonic behavior is observable when the electric field is polarized parallel to the wires, resulting in a frequency-dependent dielectric response as predicted analytically and numerically; see Fig. 2 and Table II. When the electric field is polarized normal to the wires, the effective dielectric constant of the composite remains very close to that of the PDMS matrix. The agreement between the predicted turn-on frequency, 2.37 THz, and the measured value, approximately 2.4 THz, in this case is remarkable, as is the agreement between the predicted match frequency, 3.10 THz, and the measured value, approximately 3.0 THz.

VII. DISCUSSION

Multilayer diffraction occurs when multiple layers of the gold strips are present. This may limit the application of the method used here to extract the optical properties, since the measurements were performed on a sample containing a single layer of gold strips. We expect that our results also apply to samples containing multiple layers of gold strips, based on our previous results in the microwave regime [20].

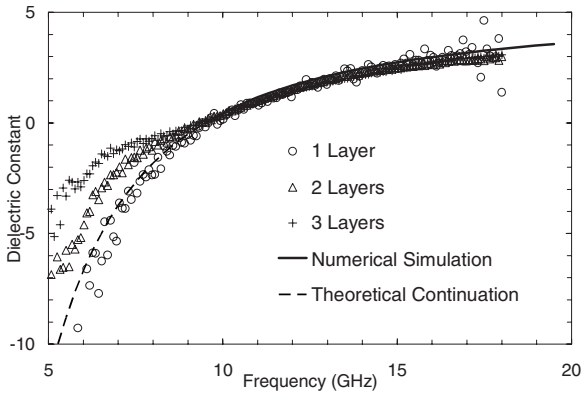

FIG. 6. Comparison of the material properties of a microwave regime plasmonic composite for single and multiple layers of wires. The solid line is the numerical prediction based on Ansoft-HFSS simulations. The dashed line is the extension of this simulation to the negative values of the dielectric constant based on Eq. (1). The agreement for the positive dielectric constant values suggests that the results of the single layer experiment may be safely extended to the multiple layer cases. The deviation among the experimental and analytical results for negative values is due to the fact that the transmitted signal in this frequency range is very small, with noise introducing large errors. (Reproduced from Ref. [21].)

A typical result is shown in Fig. 6. This is a reproduction of Fig. 12.4(d) from Ref. [20]. The samples consisted of an Epoxy/Glass Fiber composite matrix with embedded copper wires. 15 cm square panels of various thicknesses were manufactured, containing bidirectional arrays of embedded 0.05 mm copper wires, spaced 3.175 mm apart in the plane of the panel and through the thickness. The three experimental results are the extracted material properties for three panels that have 1, 2, and 3, embedded copper wire arrays. The material properties were not extracted using the Kramers-Kronig relations, but rather by the direct measurement of the phase and magnitude of the transmitted wave. For each case (1, 2, or 3 layer samples) the transmission magnitude and phase were used to calculate the permittivity of the sample, based on the iterative search procedure explained earlier. These are compared with the results from numerical calculations, based on frequency domain simulation of a single unit cell, and the theoretical continuation of the dielectric constant to negative values based on Eq. (1). The observed agreement among the results for positive values of the dielectric constant is remarkable. The deviation in the range of the negative values of the dielectric constant is due to the presence of large absorption and reflection, resulting in very small transmission, with the noise introducing large errors. Specifically, as the permittivity approaches zero around the turn-on frequency, the measured transmission diminishes substantially. Therefore, the extraction procedure would inherently have large errors due to the amplified effect of the noise. As discussed in the introduction, we expect that the micron-scale multiple layer samples show the same behavior at terahertz frequencies as similar millimeter-scale composites do in the microwave regime. The dimensionless ratio of the free space wavelength at the plasmon frequency to the layer thickness λ_p/s in the microwave regime composites is

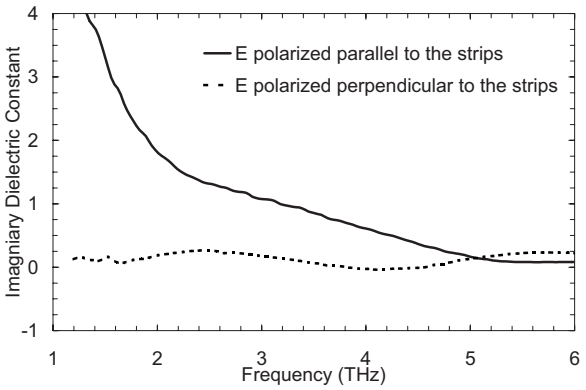

FIG. 7. The extracted imaginary part of the dielectric constant. The real parts are shown in Fig. 5.

9.9 compared to 6.25 in the terahertz regime samples. This indicates that the response of the two designs for multiple layer samples must be relatively the same. The agreement between the homogenized material properties from single and multiple layers at microwave frequencies suggests a similar agreement should exist at higher frequencies for geometrically similar structure of smaller scale. It must be noted here that for a large segment of the measured frequency band, our analysis suggests considerable losses for the plasmonic response; see Fig. 7. Although the imaginary part of the dielectric constant of the host material, PDMS, can be quite large (up to 0.21; see Fig. 3), we attribute this to strong resistive losses against currents in the nanostrips. This clearly limits the potential applications of such composites.

VIII. CONCLUSIONS

This work demonstrates that thin wire arrays can be embedded in a host material to create artificial effective plasmonic media in the far-infrared terahertz frequency regime. Both numerical design and analysis provide reliable predictions throughout this range. New methods of fabrication and measurement were developed to create and characterize the samples, and the effective electromagnetic properties of the composite were successfully extracted.

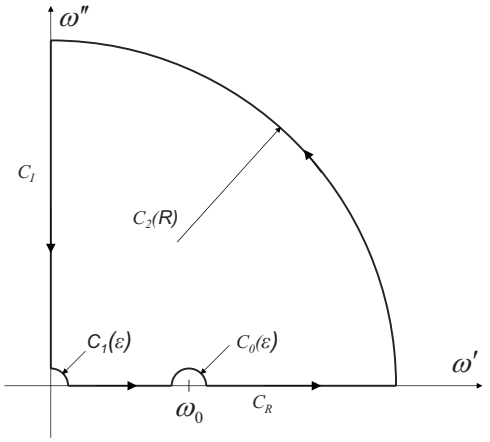

FIG. 8. Integration contour used for derivation of the complex argument of the transmission coefficient from its magnitude.

ACKNOWLEDGMENTS

This work has been supported by ARO DAAD19-00-1-0525 to the University of California, San Diego and by DARPA award no. HR00011-04-1-0053 to Harvard University. The authors wish to thank David R. Smith for many fruitful and illuminating discussions.

APPENDIX

A causal transmission coefficient in any structure, $E_t(\omega) = T(\omega)E_i(\omega)$, has no poles in the upper half of the frequency plane. Also, one can prove from physical considerations that, in this domain, $T(\omega)$ is real (and positive) only on the positive imaginary axis [21,22]. Furthermore, $T(\omega)$ is nonzero except as $|\omega| \to \infty$ and possibly as $|\omega| \to 0$.

If the magnitude of $T(\omega)$ is known on the entire positive real axis, the above conditions make it possible to calculate its complex argument on this axis. To do this, consider the integral $I = \oint_C \frac{\ln T(\omega)}{\omega^2 - \omega_0^2} d\omega$ on the contour shown in Fig. 8 ($\varepsilon \to 0, R \to \infty$). The integral is zero since the integrand has no poles inside the contour. Consider the real part of this integral on the five segments shown in Fig. 7. On C_0, $I_{C_0} = \frac{-i\pi}{2\omega_0}[\ln|T(\omega_0)| + i\theta(\omega_0)]$, therefore

$$\mathrm{Re}(I_{C_0}) = \frac{\pi}{2\omega_0}\theta(\omega_0). \tag{8}$$

On C_I, $\mathrm{Im}[T(i\omega'')] = 0$ and $\mathrm{Re}[T(i\omega'')] > 0$. Therefore $\theta(i\omega'') = 0$, and

$$\mathrm{Re}(I_{C_I}) = \mathrm{Re}\left(\int_\infty^0 - \frac{\ln|T(i\omega'')|}{\omega''^2 + \omega_0^2} d(i\omega'') \right) = 0. \tag{9}$$

On C_1 one can prove for a plasmonic dielectric constant that

$$\lim_{\varepsilon \to 0} \mathrm{Re}(I_{C_1}) = 0. \tag{10}$$

By a similar argument, one can show that the real part of the integral on C_2 is

$$\mathrm{Re}(I_{C_2}) = -\frac{\pi^2}{2} d_f. \tag{11}$$

Adding all these segments and solving for $\theta(\omega_0)$ from $\mathrm{Re}(I) = 0$, we obtain

$$\theta(\omega_0) = \pi\omega_0 d_f - \frac{2\omega_0}{\pi} P \int_0^\infty \frac{\ln|T(\omega)|}{\omega^2 - \omega_0^2} d\omega, \tag{12}$$

where P denotes the Cauchy principal value.

This integral, although bounded and well-defined, is difficult to evaluate numerically, since the integrand is unbounded near ω_0. It can be rewritten as

$$\theta(\omega_0) = \pi\omega_0 d_f - \frac{2\omega_0}{\pi} P \int_0^\infty \frac{\ln|T(\omega)/T(\omega_0)|}{\omega^2 - \omega_0^2} d\omega. \tag{13}$$

The integrand in this case is bounded near ω_0. If the measurement interval is $[\omega_m, \omega_M]$, then

$$\theta(\omega_0) = \pi\omega_0 d_f - \frac{2\omega_0}{\pi} \left[\int_0^{\omega_m} + P \int_{\omega_m}^{\omega_M} + \int_{\omega_M}^{\alpha} + \int_{\alpha}^{\infty} \right], \tag{14}$$

where $\alpha \gg \omega_0$ is a large arbitrary value. After appropriate approximations for each segment, the correct argument of the transmission coefficient can be calculated.

[1] R. N. Bracewell, *Wireless Engineer* (Iliff and Sons Ltd., London, 1954), p. 320.
[2] W. Rotman, IRE Trans. Antennas Propag. **10**, 82 (1962).
[3] J. B. Pendry, A. J. Holden, W. J. Stewart, and I. Youngs, Phys. Rev. Lett. **76**, 4773 (1996).
[4] S. C. Nemat-Nasser, A. V. Amirkhizi, T. A. Plaisted, J. B. Isaacs, and S. Nemat-Nasser, Proc. SPIE **4698**, 237 (2002).
[5] R. Ulrich, Infrared Phys. **7**, 37 (1967).
[6] R. Ulrich, Infrared Phys. **7**, 65 (1967).
[7] R. Ulrich, Appl. Opt. **39**, 1987 (1968).
[8] H. A. Smith, M. Rebbert, and O. Sternberg, Appl. Phys. Lett. **82**, 3605 (2003).
[9] I. Puscasu, D. Spencer, and G. D. Boreman, Appl. Opt. **39**, 1570 (2000).
[10] D. Wu, N. Fang, C. Sun, X. Zhang, W. J. Padilla, D. N. Basov, D. R. Smith, and S. Schultz, Appl. Phys. Lett. **83**, 201 (2003).
[11] T.-J. Yen, D. Wu, N. Fang, and X. Zhang, Proc. SPIE **5512**, 100 (2004).
[12] *Ansoft HFSS 8.0 User Documentation* (Ansoft Corporation, 2000).
[13] W. Bruns, IEEE Trans. Magn. **32**, 1453 (1996).
[14] N. Bowden, S. Brittain, A. G. Evans, J. W. Hutchinson, and G. W. Whitesides, Nature (London) **393**, 146 (1998).
[15] J. N. Lee, C. Park, and G. M. Whitesides, Anal. Chem. **75**, 6544 (2003).
[16] F. Wooten, *Optical Properties of Solids* (Academic Press, New York, 1972).
[17] S. Maeda, G. Thyagarajan, and P. N. Shatz, J. Chem. Phys. **39**, 3474 (1963).
[18] E. J. Singley, K. S. Burch, R. Kawakami, J. Stephens, D. D. Awschalom, and D. N. Basov, Phys. Rev. B **68**, 165204 (2003).
[19] S. Ramo and J. R. Whinnery, *Fields and Waves in Modern Radio* (Wiley, New York, 1953).
[20] S. Nemat-Nasser, S. C. Nemat-Nasser, T. A. Plaisted, A. Starr, and A. V. Amirkhizi, in *Biomimetics: Biologically Inspired Technologies*, edited by Y. Bar-Cohen (CRC Press, Boca Raton, FL, 2006) pp. 309–341.
[21] L. D. Landau and E. M. Lifshitz, *Statistical Physics, Part 1*, third edition (Butterworth-Heinemann, Oxford, UK, 1984).
[22] L. D. Landau and E. M. Lifshitz, *Electrodynamics of Continuous Media*, second edition (Butterworth-Heinemann, Oxford, UK, 1984).